Dynamics of solidification in Al thin films measured using a nanocalorimeter

P. Swaminathan, D. A. LaVan, and T. P. Weihs

Citation: Journal of Applied Physics **110**, 113519 (2011); doi: 10.1063/1.3668128
View online: http://dx.doi.org/10.1063/1.3668128
View Table of Contents: http://scitation.aip.org/content/aip/journal/jap/110/11?ver=pdfcov
Published by the AIP Publishing

Dynamics of solidification in Al thin films measured using a nanocalorimeter

P. Swaminathan,[1,2] D. A. LaVan,[2,a)] and T. P. Weihs[1,a)]
[1]*Department of Materials Science and Engineering, Johns Hopkins University, Baltimore, Maryland 21218, USA*
[2]*Ceramics Division, Material Measurement Laboratory, National Institute of Standards and Technology, Gaithersburg, Maryland 20899, USA*

(Received 19 April 2011; accepted 11 November 2011; published online 9 December 2011)

We demonstrate how a nanocalorimeter can be used to measure the dynamics of thin film melting and solidification using aluminum as a model system. Recalescence, a rise in temperature due to enthalpy release on solidification, is observed when the rate of heat release is faster than the rate of heat extraction. For thin films, with a large density of nucleation centers at the interface, recalescence effects are observed at high cooling rates where direct measurements of heat capacities and enthalpy changes are challenging. Temperature rates of 10^4 K/s were applied using nanocalorimeter chips; the nanocalorimeter allows direct measurement of the under cooling, temperature rise during solidification, and the associated changes in enthalpy. This work highlights some of the challenges recalescence causes in physical measurements and provides a numerical strategy to evaluate enthalpy changes during rapid solidification. © *2011 American Institute of Physics*. [doi:10.1063/1.3668128]

I. INTRODUCTION

Measuring the dynamics of rapid transitions, such as solidification of thin films is of crucial importance to the understanding of the physical properties of condensed matter. During solidification a certain degree of undercooling occurs before the solid phase starts to nucleate from the molten phase. As the solid grows it releases the enthalpy of solidification, which can cause an abrupt rise in temperature of the material, a phenomenon known as recalescence.[1–5] Recalescence occurs when the heat release on solidification is faster than the rate of heat extraction from the sample. Faster cooling rates can lead to higher heat release rates due to delayed nucleation and larger undercooling;[6] this regime is frequently encountered in thin films and nanomaterials due to their small mass, but is balanced against the high interfacial areas in these materials that tend to favor easier nucleation. During recalescence, the maximum temperature rise cannot exceed the melting point of the material.[1] This opens the possibility of defining melting point reference values of pure materials in terms of dynamic measurements, an especially useful approach for high rate measurements on samples, such as thin films.

Temperature rise during rapid solidification has been observed in semiconductor thin films melted by ultrafast laser pulses. Because of the short time scales involved (order of nanoseconds), recalescence was observed indirectly by measuring changes in reflectivity during melting.[7–9] Other techniques involve electromagnetic levitation to isolate a sample and delay nucleation with high speed cameras to capture solidification fronts and recalescence.[10–12] However, none of these observations can quantify the enthalpy changes associated with these transformations; there is a need to understand and quantify the enthalpy changes at rapid solidification rates.

We show how a nanocalorimeter can be used for this purpose, using the melting and solidification of an Al thin film as a model system. We also highlight some of the difficulties associated with the dynamic analysis to calculate enthalpy change during solidification and methods to overcome these difficulties.

A nanocalorimeter is a micromachined device; our nanocalorimeter chips consist of a thin strip of Pt suspended on a SiN_x membrane on a Si frame.[13–15] The Pt serves as both the heater and temperature sensor and the material to be measured is deposited onto the membrane. The extreme sensitivity of the nanocalorimeter allows observation of heat capacity changes on the order of tens of nJ/K at heating rates as high as 10^6 K/s,[16] and addresses dynamic measurements of heat capacities and phase transformations.[17–20]

II. EXPERIMENTAL DETAILS

The steps involved in fabrication of the nanocalorimeter have been described in detail elsewhere.[14] The chips are calibrated by local Joule heating of the Pt strip and recording the Pt resistance using the 4-wire measurement while measuring temperature using a pyrometer.[21] The Al thin film is deposited on the center of the membrane, on the SiN_x side, by e-beam evaporation using a custom designed shadow mask.[22] A schematic of the nanocalorimeter, with the different layers, is shown in Fig. 1. The base pressure during deposition is less than 5×10^{-6} Torr. The Al film is 50 nm thick (deposition rate 0.1 nm/s) and is capped on both sides with a 10 nm Al_2O_3 film. The uniformity of the film thickness in this deposition system, measured with a mechanical profilometer on 200 nm thick test films, is 3.8%.

After deposition, the chips are transferred into a system with base pressure of less than 5×10^{-7} Torr. Measurements

a)Authors to whom correspondence should be addressed. Electronic addresses: david.lavan@nist.gov and weihs@jhu.edu.

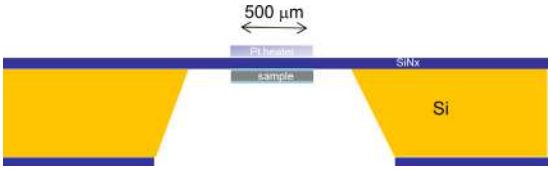

FIG. 1. (Color online) Cross section of a nanocalorimeter chip. The SiN_x layer is 100 nm thick and grown by low pressure chemical vapor deposition to generate a low stress film that with slightly tensile residual stress. The 500 μm wide Pt heater is patterned on the front of the device and deposited using e-beam evaporation; a titanium adhesion layer is used. The Al sample is deposited on the reverse side, using a shadow mask, and is sandwiched between layers of Al_2O_3. The Al and Al_2O_3 layers were also deposited using e-beam evaporation.

are performed in the differential mode using a bare chip as a reference.[23] The sample and reference chip are heated with a 20 ms current pulse. They are monitored for an additional 180 ms to record cooling. Data are acquired every 10 μs. The current pulse causes the sample chip to reach a peak temperature of 973 K (ITS-90 value for bulk Al melting is 933.15 K, Ref. 31) and completely melt the Al film. In order to ensure that there are no microstructural changes (in the form of grain growth or alloying with the substrate) during heating, 30 consecutive cycles of heating and cooling are performed, with a 2 s delay between cycles. The data from the first 10 cycles were not used and the data from the remaining 20 were averaged after examining then individually to ensure that there were no systematic fluctuations in melting and solidification temperatures.

III. RESULTS AND DISCUSSION

The heating and cooling data for the sample and reference are shown in Fig. 2(a). The temperature of the reference chip changed monotonically during heating and cooling. For the chip containing the sample, the heating rate slowed during melting and then increased once melting was completed. During cooling, the release of the heat of solidification caused the temperature to rise briefly. The sharp peak seen in Fig. 2(a) at 20 ms (in both sample and reference) represents the discontinuity in measurement when the instrument switches from heating cycle to cooling cycle (the applied current must be reduced to transition to cooling; some current must be applied during cooling to measure resistance and temperature). Figure 2(b) shows a portion of the heating and cooling data for the sample chip, with the horizontal dotted line representing the bulk Al melting point. The duration of melting is approximately 5 ms; this value is related to the propagation rate for 1 (or a small number) of melting fronts. Finite element modeling of temperature gradients in the chip during heating shows that there is a central region covering a majority of the sensitive area at the maximum temperature; temperature decreases toward the sides and edges of the heater.[21,24] Because of these temperature gradients, melting would likely initiate in the central region and spread outward. Recalescence occurs with the sharp rise in temperature of the sample during cooling. Dendritic solidification velocities in Al for low undercooling are of the order of 1 m/s.[25] For our Al film, the observed undercooling is approximately 15 K or 1.6% on an absolute scale. Given that the length of the Pt heater/sensor where measurements are conducted is 6 mm, this length scale would mean that the approximate time for a single melting front to propagate along the strip would be 6 ms, which is close to the time observed in Fig. 2(b).

In order to check the effectiveness of the analysis procedure and the uncertainty in heat capacity measurement we looked at heating and cooling data from a bare chip (prior to deposition of the Al) under the same conditions as the experiment. The temperature data in Fig. 2 is analyzed to extract the heating and cooling rate.[23] Direct differentiation of the temperature versus time data is noisy, especially during cooling, and hence the above analysis makes use of the heating/cooling in the reference chip (which is monotonic) and the differential signal (which has less noise) to obtain the heating/cooling rate in the sample chip. Working in high vacuum, heat losses are conductive and radiative. From the dT/dt data we can calculate the apparent heat capacity of the bare chip during cooling and compare it with the apparent heat capacity during heating. The two values should be the same but our calculations show that there is a difference of 20% in the heat capacities above 700 K and a large discrepancy at lower temperatures. The difference arises from the fact that temperature measurements in the nanocalorimeter are carried out by measuring small changes in resistances at high rates. In the cooling cycle, the applied current is an order of magnitude lower than typical currents in the heating cycle which leads to greater noise in the temperature data (typical current during heating is 30 mA, during cooling it is 2 mA) which propagates through the calculations leading to greater uncertainty in the heat capacity and enthalpies calculated from cooling data. For comparison, a typical differential scanning calorimeter (DSC), has an uncertainty in the heat capacity measurement of around 2.5%,[26] due in part to the thermal lag between the temperature sensor, sample pan, and the actual sample.[1] In a nanocalorimeter with an intimately deposited sample, there is no thermal discontinuity between the sample and the heater/sensor[21] and no sample

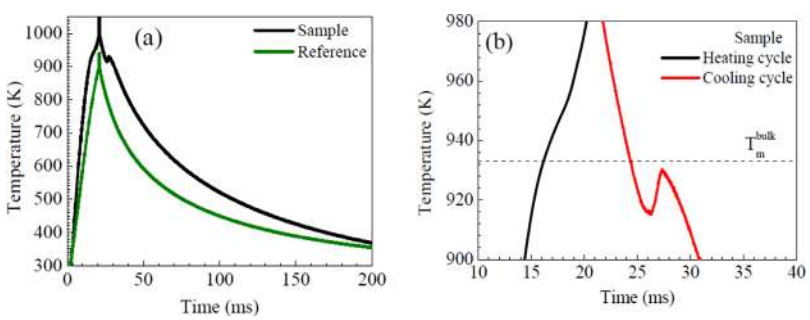

FIG. 2. (Color online) (a) Plot of temperature vs time for the sample and reference chip. Current is applied for 20 ms (heating), and the cooling is observed for an additional 180 ms. This plot is an average of 30 consecutive measurements, with a 2 s pause between subsequent measurements. (b) A portion of the same temperature vs time plot showing melting in the heating cycle and the temperature rise during cooling due to recalescence. The duration of melting is given by the change in slope of the temperature plot and is approximately 5 ms. The duration of solidification is seen more clearly by the rise in temperature and is 2.0-2.6 ms.

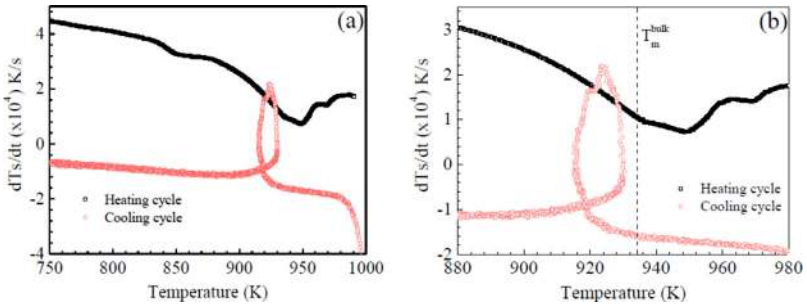

FIG. 3. (Color online) (a) dT_s/dt vs temperature during the heating and cooling. During heating, dT_s/dt approaches 0 as the aluminum film starts to melt, but returns to the original rate once melting is complete. During the cooling cycle, dT_s/dt starts out negative, and changes to positive during recalescence. Once solidification is complete the rate returns to the original trend. The recalescence portion is expanded in (b). The solidification process starts around 928 K; dT_s/dt becomes positive at 913 K, the lowest temperature seen during the recalescence cycle. The maximum temperature reached during the recalescence cycle is 931 K.

pan but additional uncertainty arises from noise sources due to the nature of the rapid measurement.

The heating and cooling rates in the sample, obtained by analysis of data shown in Fig. 2, are plotted as a function of temperature in Fig. 3(a). The behavior in the region around the melting point is shown in Fig. 3(b). Heating slows at the onset of melting and continues until melting is complete; the heating rate increases at the end of melting and the molten sample reaches a maximum temperature of 973 K. The cooling rate is governed primarily by heat loss from the chip and is on the order of 10^4 K/s, which is slightly lower than the heating rate. During cooling, the temperature initially decreases, shown by the initial negative slope of dT/dt. As molten Al starts to solidify the enthalpy of solidification is released, which momentarily reverses the cooling process. The temperature at which solidification starts from the liquid state (some undercooling is expected) is 928 K. Temperature continues to decrease, with a slower rate, until 913 K when dT/dt shifts from negative to positive as the heat released exceeds heat loss and causes a rise in temperature. The peak temperature achieved during the recalescence heating cycle is 931 K. The maximum increase in temperature during recalescence is from 913 K to 931 K, i.e., 18 K. Once solidification is complete the sample cools to room temperature. There is a smaller trough seen in the heating cycle around 843 K [see Fig. 3(a)]. It is possible that this trough is due to minor intermixing of Al and Si (Ref. 27) (from SiN_x) across the Al_2O_3 layer, but we do not see the peak increasing in subsequent cycles. Also, we do not see cycle to cycle shifts in the melting and recalescence temperatures or changes in peak height (as we would expect for oxidation or mixing). It is possible that prolonged temperature cycling can cause the Al film to dewet and depending upon the size of the islands, could change the degree of undercooling and broaden the melting and solidification peaks. We cannot completely rule out dewetting, though the time the film spends close to the melting point is of the order of ms and the film is capped with Al_2O_3, but we do not see peak broadening during the 30 heating and cooling repetitions we collect in one experiment. To ensure that minor microstructural changes from the as-deposited to thermally cycled state do not affect the enthalpy calculations, we only average data from the last 20 cycles; averaging is used to reduce noise. We also examined the data from each cycle individually.

In order to quantify the changes in enthalpies, heat losses must be subtracted from the total heat input to the sample. Applied power and heat loss data for the heating and cooling cycles are plotted as a function of temperature in Fig. 4. The applied power is calculated from the measured resistance and current to the Pt heater/sensor. The difference between the heating and cooling cycles is as expected and is due to differences in the applied current. The sources of heat loss are limited to conduction and radiation which are a function of the temperature difference between the calorimeter and the ambient, modeled using[23]

$$W_L = A + C_c(T - 298) + C_R(T^4 - 298^4), \tag{1}$$

where W_L is the heat loss from the calorimeter, T is the chip temperature in K, and A, C_c, and C_R, are fit parameters. In order to obtain these fit parameters we use the bare chip measuring applied power and heating rates for pulses of different duration.

The applied power (P_s), heat loss (W_L), heating rate (dT_s/dt), and heat capacity (C_p) of a nanocalorimeter chip are related by[23]

$$C_p \frac{dT_s}{dt} = P_s - W_L. \tag{2}$$

Since W_L depends only on temperature differences we can eliminate it using current pulses of different durations (different heating rates) over the same temperature range. The heat capacity is then given by

$$C_p = \frac{(P_s)_1 - (P_s)_2}{(dT_s/dt)_1 - (dT_s/dt)_2}, \tag{3}$$

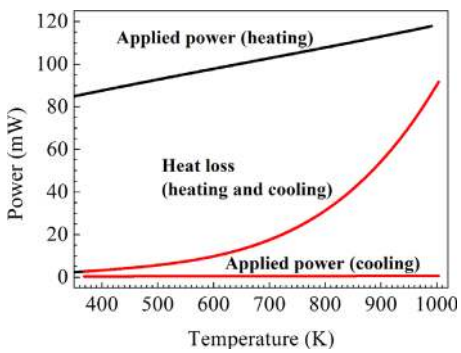

FIG. 4. (Color online) Applied power and calculated heat losses in the sample chip, during heating and cooling. The nanocalorimeter operates in vacuum; the heat losses arise from conduction and radiation and are a function of temperature, but not rate. The losses are modeled using Eq. (1) and the heat loss coefficients are obtained from baseline measurement to correct subsequent measurements. The applied power during cooling is much less than the applied power during heating; some power must be applied to measure temperature with this nanocalorimeter.

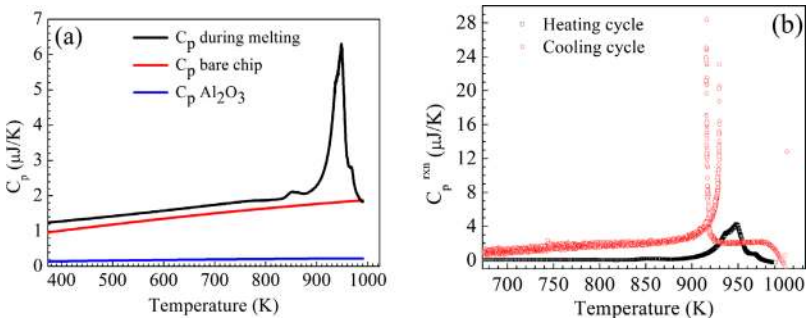

FIG. 5. (Color online) (a) Gross apparent heat capacity of the sample and chip during Al melting. The plot also includes the heat capacity of the bare chip and the Al_2O_3 layer (obtained during baseline calibration). (b) Net apparent heat capacity of the Al film during heating and cooling. The cooling cycle data is discontinuous because the heating rate shifts from negative to positive (see Fig. 3).

where $(P_s)_1$ and $(P_s)_2$ are values of applied power for two different current pulses and $(dT_s/dt)_1$ and $(dT_s/dt)_2$ are their respective heating rates. The heat capacity from Eq. (3) can be substituted back into Eq. (2) to obtain the heat loss. We perform these baseline measurements using current pulses of 8, 10, 16, and 20 ms duration; on a bare chip and a chip containing only alumina (to more closely capture the surface emissivity in the true experiment). The data for the baseline measurements were averaged with 100 repetitions for each pulse time to reduce noise. The heat losses are fitted with Eq. (1) to obtain the coefficients A, C_c, and C_R. These coefficients are then used to calculate the heat losses during the actual experiment. This heat loss is shown in Fig. 4 along with the applied power.

The heat capacity of the sample nanocalorimeter chip (C_p^{chip}) during heating, calculated using Eq. (2), is shown in Fig. 5(a). The heat capacity consists of three parts and is given by

$$C_p^{chip} = C_p^{rxn} + C_p^{barechip} + C_p^{Al_2O_3}, \tag{4}$$

where C_p^{rxn} is the heat capacity associated with melting, $C_p^{barechip}$ and $C_p^{Al_2O_3}$ are the heat capacities of the chip (Pt and SiN_x) and the Al_2O_3 layers, respectively. These later values were obtained during the baseline measurements as described above. Figure 5(a) shows the total heat capacity and the contributions from the bare chip and the alumina layer. As one check of the measurement, the increase in the room temperature apparent heat capacity and the molar heat capacity for bulk Al were compared. Based on the apparent heat capacity, the film thickness was calculated to be 46.8 nm, which is within 6% of the nominal value (50 nm).

Subtracting the heat capacity of the bare chip and alumina from the total heat capacity gives the heat capacity of the reaction (C_p^{rxn}) and this is plotted for the heating and cooling cycle in Fig. 5(b) and includes the contribution from the heat capacity of solid and liquid Al. The discontinuity in the cooling data arises because the heat capacity is inversely proportional to dT/dt, see Eq. (2), and dT/dt during cooling changes from negative to zero to positive during cooling (as heat is released during recalescence) and then back to zero and negative (once solidification stops). The zero-crossings result in numerical singularities in the derived heat capacity on cooling.

The area under the heat capacity curve gives the total enthalpy of the reaction. This can be expressed mathematically as

$$\Delta H_{rxn}{}_{t1}^{t2} = \sum_{t1}^{t2} C_p^{rxn} \frac{dT_s}{dt}(t)\Delta t, \tag{5}$$

where $\Delta H_{rxn}{}_{t1}^{t2}$ refers to the total amount of heat released (absorbed) between the time period $(t_2 - t_1)$, C_p^{rxn} is the "heat capacity" of the reaction, $dT_s/dt(t)$ is the heating rate, which is a function of time, and Δt is 10 μs. The enthalpies of reaction for the heating and cooling cycle are shown in Fig. 6(a). While Eq. (5) can be applied directly for the heating cycle the discontinuities in C_p^{rxn}on the cooling cycle precludes direct application and lead to discontinuities in the enthalpy (boxed regions in Fig. 6(a)). For the cooling cycle Eq. (5) can be modified using Eq. (2) and Eq. (4) as given below

$$\begin{aligned}
C_p^{rxn} &= C_p^{chip} - C_p^{barechip} - C_p^{Al_2O_3},\\
C_p^{chip} &= \frac{P_s - W_L}{dT_s/dt}\\
C_p^{rxn} &= \frac{P_s - W_L}{dT_s/dt} - (C_p^{barechip} + C_p^{Al_2O_3}),\\
\Delta H_{rxn}{}_{t1}^{t2} &= \sum_{t1}^{t2} C_p^{rxn}\frac{dT_s}{dt}\Delta t\\
&= \sum_{t1}^{t2}\left(P_s - W_L - (C_p^{barechip} + C_p^{Al_2O_3})\frac{dT_s}{dt}\right)\Delta t.
\end{aligned} \tag{6}$$

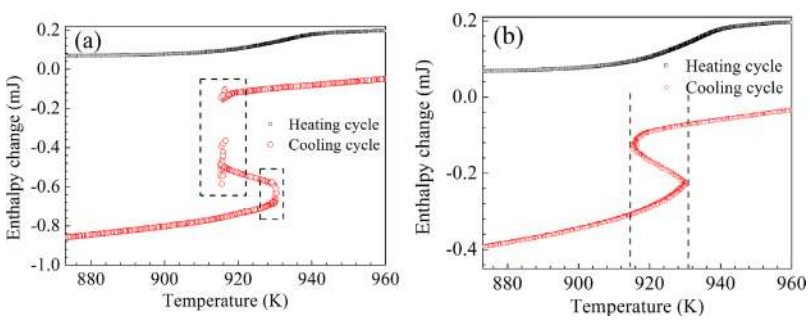

FIG. 6. (Color online) (a) Enthalpy as a function of temperature for the heating and cooling cycles, calculated using Eq. (5). The discontinuity in the heat capacity during cooling [see Fig. 5(b)] produces discontinuities in the calculated enthalpy (boxed regions). The measured change in enthalpy on heating from room temperature to 973 K is 0.194 mJ. The total heat absorbed during melting is 0.136 mJ. (b) Enthalpy calculated using modified approach, shown in Eq. (6). This modification avoids the discontinuities and provides a reasonable quantification of the change in enthalpy during cooling.

By removing dT_s/dt from the denominator, this modification removes the singularities in the cooling cycle and the correct enthalpy change during cooling is plotted in Fig. 6(b). Thus, for studies of solidification behavior using the nanocalorimeter, in cases where recalescence effects cause temperature reversals and numerical discontinuities, direct integration of heat capacity to obtain enthalpy of freezing cannot be used.

The enthalpy change during heating represents a solid phase melting in a finite time interval. The enthalpy change during cooling includes the rise in temperature due to recalescence. If the freezing takes place isothermally, as in slow near-equilibrium freezing, the enthalpy versus temperature plot will be a vertical line separating the solid and liquid phases, representing the enthalpy of fusion.[28] The other extreme occurs under isenthalpic or adiabatic freezing, when nucleation of the solid is suppressed until the liquid enthalpy is lowered by an amount equal to (or greater than) the heat of fusion. In this case complete solidification occurs very rapidly by the end of recalescence without external heat loss and the maximum temperature rise is to the melting temperature of the material.[29] The present experiments represent an intermediate between these two extremes, where further heat extraction is required to complete solidification after recalescence.

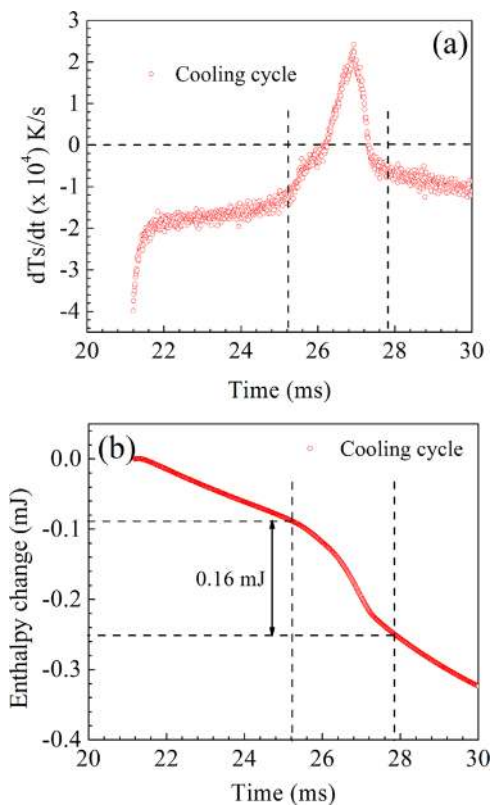

FIG. 7. (Color online) (a) dT_s/dt as a function of time in the cooling cycle. The vertical markers indicate start and end of solidification. The start time is 25.2 ms, chosen based on when dT_s/dt starts to increase (see marker in Fig. 3(b)). The end of the solidification was set at 27.8 ms, based on the change in slope of dT_s/dt. If we set the end of solidification as the moment when dT_s/dt becomes negative, the value would be 27.2 ms. The actual solidification point likely lies within this 600 μs window. (b) Enthalpy change as a function of time during cooling and solidification. The measured heat released during solidification is 0.16 mJ (for solidification interval 25.2 – 27.8 ms) which is 15% higher than the measured enthalpy of melting. For the solidification interval 25.2 – 27.2 ms, the measured enthalpy released would be 0.13 mJ, 4% lower than the measured enthalpy of melting.

The total amount of heat absorbed from room temperature to 973 K was found to be 0.194 mJ, obtained by calculating the area under the C_p plot and could also be found directly from the enthalpy plot in Fig. 6(b). This also includes the heat capacity contributions from solid and liquid aluminum. The heat absorbed during melting (enthalpy) was 0.136 mJ. From the area of the film (6 mm $\times$ 0.5 mm), calculated film thickness from heat capacity increase (46.8 nm), density (2.7 g cm^{-3}), molar mass (26.98 g mol^{-1}), and the measured enthalpy (0.136 mJ), the calculated molar enthalpy for melting was 9.68 kJ mol^{-1}. The molar enthalpy reported for melting of pure bulk Al is 10.58 $\pm$ 0.15 kJ mol^{-1},[30] a difference of 8.5%. In addition to experimental uncertainty this difference may be associated with a variation in the as-deposited thickness or a difference in the heat capacity of e-beam deposited Al thin film compared to the bulk.

To evaluate the enthalpy release during cooling, we consider the enthalpy change as a function of time, plotted along with the heating rate as a function of time in Fig. 7. The starting point for solidification was taken as the moment when dT/dt starts to increase during cooling. This occurs at 25.2 ms in our data set (the cooling cycle starts at 20 ms). If we define the point where solidification is complete as the moment when the cooling rate returns to the gradual negative value, the end point is at 27.8 ms. Based on this value, the recalescence event lasts approximately 2.6 ms. The total amount of heat released during this process, from Fig. 7(b), is 0.16 mJ, which is 15% higher than the enthalpy obtained during melting (0.136 mJ). At the other extreme, if completion is taken as the moment when dT/dt becomes negative, the time value is 27.2 ms and the total heat release is 0.13 mJ, which is 4% lower than the enthalpy obtained during melting. The actual time when solidification is complete lies within this 600 μs window. If we select a time that lies at the center of this window (27.5 ms), the measured enthalpies of melting and solidification are equal.

The ITS-90 value for Al is based on a freezing point measurement at very slow cooling rates.[31] For rapid heating and cooling processes, we expect shifts in the heating and cooling curves from equilibrium. One such shift can be seen in the cooling curve of Fig. 3(b), where solidification starts below 928 K. Also, in the nanocalorimeter, the temperature is averaged over the sensitive area of the heater which results in broadening of the melting and solidification peaks. Small temperature gradients at the ends and edges of the heater have been shown with finite element modeling.[21,24]

During solidification, the maximum temperature reached during recalescence may serve as a useful reference value for dynamic measurements since the heat released due to the enthalpy of solidification cannot heat the sample past the melting point of the material[1,29] and the "arrest" seen at the peak of recalescence serves as an indication that the material reached the onset of melting. From a pragmatic perspective, this heat source is internal to the material with perfect thermal contact and the heat released during solidification is distributed broadly across the sample given that there are ample opportunities for heterogeneous nucleation. As shown in

Fig. 3(b), the maximum temperature reached during recalescence is 931 K (within 0.2% of the ITS-90 value[31]).

IV. CONCLUSION

In summary, we have measured the melting and recalescence of an Al thin film using a nanocalorimeter. The fast heating and cooling rates and high sensitivity of the nanocalorimeter allow direct measurement of recalescence. The rise in temperature during cooling results in numerical singularities during calculation of heat capacities and requires changes to the analysis approach. Melting initiates at one (or a few) locations and progresses across the chip; solidification initiates at many locations and progresses faster across the sample. The maximum temperature rise during recalescence cannot exceed the melting point of the material and is a potential reference value for dynamic thermal measurements.

ACKNOWLEDGMENTS

Research is supported in part by NIST Grant No. 70NANB9H9146. Research is performed in part at the NIST Center for Nanoscale Science & Technology. Certain commercial equipment, instruments, or materials are identified in this document. Such identification does not imply recommendation or endorsement by the National Institute of Standards and Technology, nor does it imply that the products identified are necessarily the best available for the purpose. We thank William Boettinger, Sara C. Barron, Ravi Kummamuru, L. H. Allen, Lito De La Rama, and Liang Hu for useful discussions and assistance.

[1]W. J. Boettinger, U. R. Kattner, K. W. Moon, and J. H. Perepezko, "DTA and Heat-Flux DSC Measurements of Alloy Melting and Freezing," NIST Special Publication No. 96-15 (U.S. Government Printing Office, Washington, DC, 2006), available online at www.nist.gov/public_affairs/practiceguides/NISTSpecial%20Pub960-15.pdf.
[2]W. L. Johnson, Prog. Mater. Sci. **30**, 81 (1986).
[3]J. H. Perepezko, *Thermal Analysis in Metallurgy*, edited by R. D. Shull and A. Joshi (TMS, Warrendale, PA, 1992).
[4]M. Baricco, L. Battezzati, and P. Rizzi, J. Alloys Compd. **220**, 212 (1995).
[5]J. H. Perepezko, Prog. Mater. Sci. **49**, 263 (2004).
[6]W. J. Boettinger and U. R. Kattner, Metall. Mater. Trans. A **33A**, 1779 (2002).
[7]S. R. Stiffler, M. O. Thompson, and P. S. Peercy, Appl. Phys. Lett. **56**, 1025 (1990).
[8]J. Siegel, J. Solis, and C. N. Afonso, Appl. Phys. Lett. **75**, 1071 (1999).
[9]J. Armengol, F. Vega, N. Chaoui, J. Solis, and C. N. Afonso, J. Appl. Phys. **93**, 1505 (2003).
[10]M. Barth, B. Wei, D. M. Herlach, and B. Feuerbacher, Mater. Sci. Eng., A **178**, 305 (1994).
[11]H. Assadi, M. Barth, A. L. Greer, and D. M. Herlach, Acta Mater. **46**, 491 (1998).
[12]H. Assadi, S. Reutzel, and D. M. Herlach, Acta Mater. **54**, 2793 (2006).
[13]D. W. Denlinger, E. N. Abarra, K. Allen, P. W. Rooney, M. T. Messer, S. K. Watson, and F. Hellman, Rev. Sci. Instrum. **65**, 946 (1994).
[14]M. Y. Efremov, E. A. Olsen, M. Zhang, F. Schiettekatte, Z. Zhang, and L. H. Allen, Rev. Sci. Instrum. **75**, 179 (2004).
[15]A. A. Minakov and C. Schick, Rev. Sci. Instrum. **78**, 073902 (2007).
[16]R. K. Kummamuru, L. D. L. Rama, L. Hu, M. D. Vaudin, M. Y. Efremov, M. L. Green, D. A. LaVan, and L. H. Allen, Appl. Phys. Lett. **95**, 181911 (2009).
[17]A. W. van Herwaarden, Thermochim. Acta **432**, 192 (2005).
[18]J. L. Garden, H. Guillou, A. F. Lopeandia, J. Richard, J. S. Heron, G. M. Souche, F. R. Ong, B. Vianay, and O. Bourgeois, Thermochim. Acta **492**, 16 (2009).
[19]W. Chen, D. Zhou, G. Xue, and C. Schick, Front. Chem. China **4**, 229 (2009).
[20]A. F. Lopeandia, E. L. Gutierrez, G. Garcia, F. Pi, A. Bernardi, A. R. Goni, M. I. Alonso, and J. R. Viejo, Mater. Sci. Semicond. Process. **9**, 806 (2006).
[21]P. Swaminathan, B. G. Burke, A. E. Holness, B. Wilthan, L. Hanssen, T. P. Weihs, and D. A. LaVan, Thermochim. Acta **522**, 60 (2011).
[22]R. K. Kummamuru, L. Hu, L. Cook, M. Y. Efremov, E. A. Olsen, and L. H. Allen, J. Micromech. Microeng. **18**, 095027 (2008).
[23]M. Y. Efremov, E. A. Olsen, M. Zhang, S. L. Lai, F. Schiettekatte, Z. S. Zhang, and L. H. Allen, Thermochim. Acta. **412**, 13 (2004).
[24]Y. Anahory, M. Guihard, D. Smeets, R. Karmouch, F. Schiettekatte, P. Vasseur, P. Desjardins, L. Hu, L. H. Allen, E. Leon-Gutierrez, and J. Rodriguez-Viejo, Thermochim. Acta **510**, 126 (2010).
[25]D. M. Herlach, Annu. Rev. Mater. Sci. **21**, 23 (1991).
[26]S. Rudtsch, Thermochim. Acta **382**, 17 (2002).
[27]J. L. Murray and A. J. McAlister, J. Phase Equilib. **5**, 74 (1984).
[28]H. B. Dong and J. D. Hunt, J. Therm. Anal. Calorim. **64**, 341 (2001).
[29]C. G. Levi and R. Mehrabian, Metall. Trans. A **13A**, 221 (1982).
[30]P. D. Desai, Int. J. Thermophys. **8**, 621 (1987).
[31]B. W. Mangum and G. T. Furukawa, "Guidelines for Realizing the International Temperature Scale of 1990 (ITS-90)," National Institute of Standards and Technology, Technical Note No. 1265 (U.S. Government Printing Office, Washington, DC, 1990), available online at www.nist.gov/customcf/get_pdf.cfm?pub_id=905199.